IEEE Access
Multidisciplinary | Rapid Review | Open Access Journal

Received December 10, 2019, accepted December 22, 2019, date of publication January 3, 2020, date of current version January 14, 2020.

Digital Object Identifier 10.1109/ACCESS.2019.2963860

Dynamic Joint Allocation of EV Charging Stations and DGs in Spatio-Temporal Expanding Grids

RACHAD ATAT[1], (Member, IEEE), MUHAMMAD ISMAIL[2], (Senior Member, IEEE), ERCHIN SERPEDIN[3], (Fellow, IEEE), AND THOMAS OVERBYE[3], (Fellow, IEEE)

[1]Department of Electrical and Computer Engineering, Texas A&M University at Qatar, Doha, Qatar
[2]Department of Computer Science, Tennessee Tech University, Cookeville, TN 38501, USA
[3]Department of Electrical and Computer Engineering, Texas A&M University, College Station, TX 77843, USA

Corresponding author: Rachad Atat (rachad.atat@qatar.tamu.edu)

This work was supported in part by the Qatar National Library, and in part by the NPRP from the Qatar National Research Fund (a member of Qatar Foundation) under Grant NPRP12S-0221-190127. The statements made herein are solely the responsibility of the authors.

ABSTRACT The number of electric vehicles (EVs) and the size of smart grid are witnessing rapid expansion in both spatial and temporal dimensions. This requires an efficient dynamic spatio-temporal allocation strategy of charging stations (CSs). Such an allocation strategy should provide acceptable charging services at different deployment stages while meeting financial and technical constraints. As new CSs get allocated, distributed generation (DG) units need to be also dynamically allocated in both space and time to compensate for the increment in the loads due to the EV charging requests. Unfortunately, existing power grid models are not suitable to reflect such spatio-temporal evolution, and hence, new models need to be developed. In this paper, we propose a spatio-temporal expanding power grid model based on stochastic geometry. Using this flexible model, we perform a dynamic joint allocation of EV CSs and DG units based on a constrained Markov decision process. The proposed dynamic allocation strategy accounts for charging coordination mechanism within each CS, which in turn allows for maximal usage of deployed chargers. We validate the proposed stochastic geometry-based power grid model against IEEE 123-bus test system. Then, we present a case study for a 5-year CSs deployment plan.

INDEX TERMS Charging stations allocation, dynamic program, electric vehicles, expanding power grid, and stochastic geometry modeling.

I. INTRODUCTION AND MOTIVATION

With the world shifting towards green solutions in an attempt to reduce carbon emissions and lessen the dependency on crude oil, the number of electric vehicles (EVs) has been witnessing a dramatic increase. While EV owners could use their household electrical system to charge their vehicles, EV charging stations (CSs) add more flexibility to the system by allowing EV owners to charge their EVs on the streets or while they are in malls or offices.

A. CHALLENGES

Several reports have indicated that the number of EVs will gradually increase over time and space [1]. This means that the load demands within the power grids due to such EVs will also increase in both spatial and temporal dimensions. Moreover, power grids are in continuous expansion in both space and time, due to the addition of new electrical buses and power lines in addition to the seasonal reconfigurations. Therefore, a dynamic spatio-temporal expanding power grid model is needed. For instance, the State of Qatar has adopted several measures for smart grid expansion with total investment cost of almost $8.5 billion, which will take place over a span of 4 years up until the next world cup in 2022 [2]. Thus, the spatio-temporal expansion of the power grid and the spatio-temporal gradual increase in the number of EVs indicate that the allocation of EV CSs should be deployed over multiple phases so as to prevent any wastage of resources. To develop a strategic and efficient deployment strategy of EV CSs, several challenges need to be addressed. First, operators cannot statically allocate EV CSs since they might end up installing too many or too few CSs. If an excess number of CSs is installed, many of these EV CSs will become underutilized, leading to unnecessary costs for installation,

The associate editor coordinating the review of this manuscript and approving it for publication was Feifei Bu.

maintenance, and operation costs of such CSs. On the other hand, if few EV CSs are deployed, a high rejection rate is expected for the EV charging demands. Even if the projected number of EVs can be known for future years, system operators shall avoid spending all the budget in the current year so as to prevent CSs from being underutilized and to keep guaranteeing acceptable service quality in the future. Hence, dynamic allocation of EV CSs needs to be performed progressively over time and space in multiple stages; otherwise a loss of profits would be expected. Indeed, a multi-stage spatio-temporal allocation of CSs shall ensure that all CSs are efficiently utilized at each stage of deployment, where only the minimum number of CSs, meeting the load demands of the current EVs' density and satisfying acceptable charging service constraints, is installed.

Second, integrating charging coordination within the planning strategy allows the maximal usage of the minimum number of deployed chargers. This presents a unique opportunity for operators to minimize the number of CSs needed to satisfy charging requirements. However, the challenge that needs to be addressed here is how to model the charging coordination mechanism within the dynamic planning strategy.

Third, with new CSs being allocated each year comes an increase in the load demands, which must be balanced with an increase in the power generation. The addition of such new generation units is to compensate for the increment in the loads due to the EV charging requests [3]. Thus, operators need a similar spatio-temporal allocation strategy for distributed generators (DGs).

B. PROPOSED SOLUTIONS

To address the aforementioned challenges, we first need a power grid model that reflects a spatio-temporal evolution. As for integrating charging coordination within the planning strategy, we need a queuing model with two priority queues at each CS: one for EVs with charging requests that can be deferred (low priority EVs) and another for EVs that require immediate charging without deferral (high priority EVs). To obtain the optimal multi-stage planning strategy, a dynamic program for joint allocation of CSs and DGs is needed.

Unfortunately, while some of the existing power grid models are dynamic [4], however they are not mapped to a geographical region, and hence spatial topological information cannot be used towards the allocation of CSs and DGs. Furthermore, existing dynamic power grid models do not follow a mathematical rule for the expansion, and hence the dynamic allocation becomes mathematically intractable. Hence, we propose a tractable generative spatio-temporal expanding power grid framework using stochastic geometry. This powerful tool allows to build a power grid model that captures the characteristics and attributes of real power grids in terms of bus degree distribution, betweenness centrality, eigen-spread, and power grid diameter. Additional benefits of using stochastic geometry include along with the ability to take into consideration the physical constraints of connecting the power grid elements as well as their spatial correlations, the ability to describe the temporal evolution of the power grid with new buses, power lines and EVs added at different time periods. Furthermore, such a model offers mathematical tractability in modeling large (city-wide) power grid structures using iterated Poisson tessellations [5]. Unlike [6], where buses are distributed in a 2D plane, our model distributes buses on roads of a Poissonian city. This makes our model more realistic and practical since buses and EVs are most likely located on linear and randomly oriented roads [7]. The stochastic geometric morphogenesis of cities utilizing iterated Poisson tessellations is in match to a high degree with the real world, as clarified in [5], [8], and [9]. Moreover, according to [10], the stochastic modeling of the actual roads with iterated Poisson tessellations was shown to be statistically equivalent to real road maps.

The national security measures practiced in many countries make it difficult to obtain spatial information about the topology of the power grid. When topological information is made available to researchers, it usually comes under strict non-disclosure agreement. This means that any obtained results cannot be shared with the research community. Since our proposed model mimics the topological characteristics and features of real power grids, the developed algorithms and methods can then be tested and applied on any actual power grid. Therefore, our model can be used as a tool for strategic planning, where for a given power grid realization, a joint dynamic tractable CSs and DGs allocation algorithm can be applied in order to obtain the number of CSs and DGs to allocate in each year and their corresponding locations.

C. RELATED WORK

Limited research is available on the allocation of CSs in smart grids. In [4], the authors used mixed-integer linear programming to solve the multi-stage joint planning and expansion of electrical distribution systems and CSs. The proposed method was verified on 18-node and 54-node distribution systems. Optimal density for CSs yielding minimal cost was derived in [11] using a unit square area. The authors then applied their model in a real city by dividing it into multiple 1 km $\times$ 1 km squares, and using data of EVs driving and charging characteristics. In [12], planning of CSs in terms of locations and service areas was carried out on an area divided into multiple sections. The analysis was based on Voronoi diagrams and branch and bound method. In [13], the authors proposed a planning method for CSs based on queuing theory using a 24-node distribution grid, taking into consideration the spatio-temporal distribution of EVs. In [14], the authors solved the joint EVs and DGs allocation problem using Genetic algorithm such that deployment and operation costs as well as green house gas emissions are minimized. The proposed allocation algorithm was tested on a 38-bus radial distribution system. In [15], the authors used a realistic network to evaluate the load demand of EVs based on realistic trips in Lyon Metropolitan area. The electric consumption of EVs is then used as an input to an integer linear program

to obtain the optimal locations of charging stations. Using particle swarm optimization algorithm, the authors in [16] solved the optimal planning of CSs by taking into account the charging demands of EVs, and the economic operation and power quality of the distribution system. The effectiveness and feasibility of the method was tested on IEEE 33-bus system. In [17], the authors used software-defined network with set-cardinality based search to allocate CSs to EVs such that their average charging time is minimized. The CSs planning problem in [18] was formulated based on game theory by taking into account the competitive charging behaviors of EVs, whose charging costs depend on other EVs' choices. The optimal allocation of CSs is obtained following the equilibrium of the EV charging game.

The works in [4], [11]–[18] suffer from the following:

- The existing works validate their proposed methods on distribution systems that are not mapped to a geographical region, and hence spatial topological information cannot be used towards the allocation of CSs.
- The algorithms tested in [11], [12], [15], [18] apply to specific cities and are not generalized to any given city.
- The existing works [11]–[14] do not present a framework for dynamic allocation of CSs that accounts for gradual increase in number of EVs over the years.
- Most of the existing works do not incorporate charging coordination mechanism within their planning framework. The accounting of such a coordination mechanism, used during system operation, within the planning framework will help to minimize the number of required chargers to satisfy the expected charging requests.

D. CONTRIBUTIONS

The contributions of this paper are summarized as follows:

- First, using tools from stochastic geometry, we model the power grid using a doubly stochastic process, namely Poisson line process (PLP) and homogeneous Poisson point process (HPPP). Such a model allows us to reflect on the spatial and temporal dimensions of the power grid expansion as well as the spatio-temporal distribution of the EVs within the power grid. The suggested model is compared with IEEE 123-bus system in terms of topological characteristics.
- Second, we obtain the average number of EVs that can be served on a specific bus. For each bus, we calculate its impact factor based on the density of EVs and the size of CSs that can be accommodated on that bus. This sets up a criterion for the allocation of CSs based on the relative importance of buses.
- Third, using a two-priority queuing model with charging coordination within the planning strategy, we obtain closed-form lower-bound expressions on the density of CSs to satisfy technical charging constraints. The obtained expressions are used to set up the dynamic program in order to obtain the minimum number of CSs and DGs to allocate at each stage of time.
- Fourth, given a predetermined budget that can be spent over a certain number of years, we formulate a multi-year joint dynamic spatio-temporal allocation strategy for CSs and DGs to satisfy certain rejection and non-idle charging constraints in an expanding power grid. We introduce an algorithm to solve the allocation problem using the constrained Markov decision process.

The remainder of this paper is organized as follows. In Section II, the stochastic-geometry based power grid model is presented. Section III presents preliminary calculations for setting up the dynamic program model. Section IV formulates and solves the finite-horizon dynamic programming allocation for CSs and DG units. Section V presents the simulation results. Finally, conclusions are drawn in Section VI. Table 1 provides a summary of notations used in the paper.

TABLE 1. Summary of notations.

Notation	Description
$\mathcal{C}$	Set of clusters
d_b	Neighbors of bus b
$\mathbb{E}\left[N_{\mathrm{EV}}^{(c)}\right]$	Average number of EVs under all buses in cluster c
$g_{b_j^{(c)}}$	Maximum number of CSs that can be installed at bus b_j
$\mathrm{IF}_{b_j^{(c)}}$	Impact factor of bus b_j in cluster c
K	Set of all bus degrees
l	Poisson line representing a road
$L_{b_j^{(c)}}$	Total load capacity of bus b_j in cluster c
$m_t^{(c)}$	Number of allocated CSs in the grid until t in cluster c
N(t)	Total number of buses at time stage t
$n_{\mathrm{b},t}$	Number of buses added at time stage t
$n_{\mathrm{CS},t}^{(c)}$	Number of CSs to allocate at t in cluster c
$n_{\mathrm{DG},t}^{(c)}$	Number of DG units to install at t in cluster c
$n_{\mathrm{EV},t}$	Number of EVs added at time stage t
P_{BT}	Blocking probability of charging requests
P_{c}	Constant power drawn by each charger
p_{cong}	Congestion charging price
p_l	Poisson line location
$P_l(t)$	Aggregate demand capacities of load buses on line l at t
$P_{\mathrm{L}}^{\mathrm{tot}}$	Aggregate load demand within the power grid
p_{norm}	Normal charging price
$P_{\mathrm{R}}(t)$	Regular load capacity at time stage t
$p_{s,s'}$	Probability that an EV accesses a CS s to get charged
R	Radius of the geographical region representing a city
$\mathcal{T}$	Set of allocation in scale of years
t_h	Time scale of hours
$x_{\mathrm{CS},t}^{(c)}$	Locations of CSs to allocate at t in cluster c
θ_l	Angle direction of the Poisson line l
λ_l	Density of the PLP Φ_l
$\lambda_{\mathrm{B}}(t)$	Density of buses HPPP Φ_{B} at time stage t
$\lambda_{\mathrm{EV}}(t)$	Density of EVs HPPP $\Phi_{\mathrm{EV}}(t)$
μ_K	Average number of edges formed by a new bus
η_i	Probabilities corresponding to different bus degrees
$\delta^{(c)}(t)$	CSs' density in cluster c at time stage t
$\lambda(t_{\mathrm{h}})$	EVs' Poisson process arrival rate
ρ	EVs' average charging service time
$\lambda^*(t_{\mathrm{h}})$	EVs' arrival rate threshold for normal pricing
χ_t	State of budget at time stage t

II. SPATIO-TEMPORAL POWER GRID MODEL

In this section, we describe the framework for developing the spatio-temporal expanding power grid model. We utilize tools from stochastic geometry to build the general topology of the power grid so as to obtain a statistical model for the planning of CSs. In order to represent roads in cities, iterated Poisson tessellations, such as PLP, can be used [5], [19]. We adopt the doubly stochastic spatial model where: i) PLP models the spatial locations of the irregular layout of roads and ii) 1D HPPP models the spatial locations of buses and EVs on each road [7], [20], [21].

We start by generating lines (i.e., roads) in a disk representing a geographical region such as a city or a town. A random number of buses following the Poisson distribution is generated on each line. Buses are then connected via power lines based on physical boundaries. Finally, load capacities are assigned to buses by matching the random load values with those of a real power grid. In addition to the spatial dimension feature of the grid, a time dimension is added to reflect the evolution of the grid over time. Let $\mathcal{T} \in \{1, \ldots, T\}$ denote time stages. In this paper, the time stage step is assumed to be one year. In each year, the number of EVs increases and the grid expands as new buses and power lines are deployed in the system. A detailed description of developing the spatio-temporal grid model is presented next.

Step 1: We start by defining a city, a town or a neighborhood as a disk $\mathcal{A}(0, R)$ with radius R. While the region under study is assumed to be circular in shape, different geometrical shapes can be assumed such as rectangular, square, etc. It is worthy to note that the geometrical shape that a region can take does not affect the power grid model, as well as the methods, algorithms, and concepts proposed in the paper. Moreover, assuming a city as a disk shape can be further justified by the spatial structures and models of American cities as discussed in [22]. In order to generate a random set of lines representing roads, we use the Poisson lines representation space, where each line ℓ_l is defined by the line angle direction $0 \leq \theta_l < 2\pi$ and by the line location $0 < p_l \leq R$. The number of lines intersecting $\mathcal{A}$ is $2\pi\lambda_l R$, where λ_l is the density of the PLP, Φ_l.

Step 2: Buses are distributed on each Poisson line $\ell_l \in \Phi_l$ following the 1D HPPP, $\Phi_{\mathrm{B},l}(t)$, with density $\lambda_{\mathrm{B},l}(t)$ at time stage t. Summing over all the lines in $\mathcal{A}$, at time stage t, the buses constitute an HPPP $\Phi_{\mathrm{B}}(t)$ with density $\lambda_{\mathrm{B}}(t) = \sum_{l=1}^{2\pi\lambda_l R} \lambda_{\mathrm{B},l}(t)$. The total number of buses, $N(t)$, in the network is expressed as $N(t) = \sum_{l=1}^{2\pi\lambda_l R} \lambda_{\mathrm{B},l}(t)|\ell_l|$, with the magnitude of the line ℓ_l being $|\ell_l| = 2R \sin\left(\cos^{-1}(p_l/R)\right)$.

Step 3: We connect buses together via power lines based on their physical paths. First, we need to figure out the immediate number of nodes, d_b, that each bus b can connect to, which is specified by the probability mass function (PMF) $f(d)$ with d denoting the bus degree. The bus degree defines the number of nodes directly connected with it. It was shown in [6] that the PMF of the degree of buses in real power grids follows the shifted sum of exponential distributions:

$$f(d) = \sum_i \frac{\eta_i}{\mu_K} e^{-\frac{d-k_i}{\mu_K}\mathbb{1}(d \geq k_i)}, \tag{1}$$

where μ_K is the average number of edges formed by a new bus; η_i are the probabilities of a node taking different values k_i of $K(t) = \{d_{b(t)} | b(t) \in (1, \ldots, N(t))\}$; and $\mathbb{1}(.)$ is the indicator function. The parameters k_i and η_i can be obtained by matching with real power grids [6].

The degree of bus b is obtained by drawing a sample, d_b, from the distribution $f(d)$. The spatial locations of d_b neighbors are found based on the Euclidean distance. Each bus b is then connected to its d_b neighbors based on the geographical boundaries and physical paths by selecting one of the potential near-geodesic routes, which were shown to be good approximations to true geodesics [23].

To ensure power delivery to every bus, disconnected buses are connected based on the shortest paths between them, such that the distribution power system achieves a radial-like network configuration structure without cycles [24].

Step 4: The final step in power grid construction is to assign load capacities to load buses. For this step, we first obtain the aggregate load demand in the power grid [25]:

$$\log[P_{\mathrm{L}}^{\mathrm{tot}}] = -0.2(\log N(t))^2 + 1.98(\log N(t)) + 0.58,$$

where $P_{\mathrm{L}}^{\mathrm{tot}}(N(t)) = \sum_{l=1}^{2\pi\lambda_l R} P_l(t)$; and $P_l(t)$ is the aggregate demand capacity of load buses on line ℓ_l at time t. Then, a random set of load capacities $[P_l(t)]_{1\times N(t)}$ is generated following the exponential distribution, while having 1% of these values falling outside the normal range (2-3 times greater) expected by the exponential distribution [25]. To assure the sum of load values remain in the range of the aggregate load capacity, we verify that $\sum_{l=1}^{2\pi\lambda_l R} P_l(t) \leq P_{\mathrm{L}}^{\mathrm{tot}}$. The load values are scaled down if this condition is not satisfied. Afterwards, we divide the node degree of each bus by the maximum node degree of all buses to obtain the normalized node degree. Similarly, we divide the load capacity of each bus by the maximum load capacity of all buses to obtain the normalized load capacity. Using the pair of normalized node degree and normalized load capacity, we obtain the 2D-PMF of a real power grid. Then, we match the real values to those of the developed ones for the corresponding buses based on their corresponding probabilities. Finally, we assign the real (unnormalized) load values to load buses based on their nodal degree [25]. In this paper, we used the load and connectivity data of IEEE test systems to assign load capacities to buses.

After the grid is initially constructed at time stage $t = 1$, we model the spatial locations of EVs on each Poisson line, $\ell_l \in \Phi_l$, following the 1D HPPP, $\Phi_{\mathrm{EV},l}(t)$, with density $\lambda_{\mathrm{EV},l}(t)$. Then, the EVs constitute an HPPP $\Phi_{\mathrm{EV}}(t)$ with density being $\lambda_{\mathrm{EV}}(t) = \sum_{l=1}^{2\pi\lambda_l R} \lambda_{\mathrm{EV},l}(t)$. At each time stage $t > 1$, a random number of buses $(n_{b,t})$ and EVs $(n_{\mathrm{EV},t})$, following the Poisson distribution, are added to the grid model. Each time a new bus b is added, we connect it to its d_b neighbors and assign it a load capacity.

Algorithm 1 explains the expansion of the buses and EVs over T years. Fig. 1 shows a sample realization of the stochastic geometry-based power grid model.

Algorithm 1 Buses and EVs Expansion Over T Years

begin
  for $t = 1 \dots T$ **do**
    ▷ Generate a random number of buses according to Poisson distribution
    $n_{(b,t)} \sim \text{Poiss}(\lambda_{\text{B},l})$
    for $i = 1, \dots n_{b,t}$ **do**
      add node i on a random Poisson line $\ell_l \in \Phi_l$
      find nearest neighbors of node i and connect the physical paths between them
      Ensure that all buses are connected without cycles
    end for
    ▷ Generate a random number of EVs according to a Poisson distribution
    $n_{(\text{EV},t)} \sim \text{Poiss}(\lambda_{\text{EV},l})$
    for $i = 1, \dots n_{(\text{EV},t)}$ **do**
      add EV i on a random Poisson line $\ell_l \in \Phi_l$
    end for
  end for
end

III. PRELIMINARY CALCULATIONS

In this section, we carry out preliminary calculations in order to set up the technical constraints of the dynamic program model in Section IV. Using all the budget in the first year to deploy CSs that are required to serve the projected number of EVs leads to underutilized and idle CSs in the current time and the near future time. Moreover, achieving acceptable rejection and non-idle levels[1] in future years might not be possible due to the temporal and spatial expansion of both the power grid and the EVs alike. Furthermore, the EVs' spatial distributions for the first year is not the same as in the last year, that is why strategic locations for CSs need to be selected. Therefore, we need to jointly allocate the minimum number of CSs and DGs in each year so that we have high utilization efficiency and low rejection of charging requests, which are all achieved with minimum deployment cost.

Towards this objective, we first begin by grouping the buses into various clusters using the k-means clustering algorithm. The idea of clustering buses is to divide the whole region into separate geographical areas (in our case 3 different areas), where the joint dynamic allocation of EV CSs and DGs can be applied to each one of them. Various areas of the planning region can have different land usage, for instance, the downtown area can have too many restaurants, shops, and parks available. This affects the charging activities and the frequency of using CSs. On the other hand, a remote less dense area might exhibit less frequent visits to CSs [26].

[1]The non-idle requirement ensures a certain utilization level of CSs.

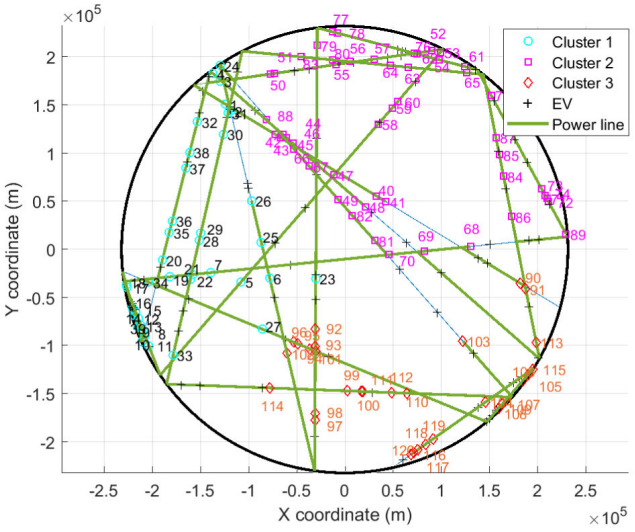

FIGURE 1. A realization example of the stochastic-geometry based power grid model with 120 buses at time stage $t = 1$, where EVs are represented by the '+' markers and other markers represent buses. Note that solid lines represent power lines and light lines represent roads.

Therefore, the clustering procedure eases the planning of CSs, as it allows operators to optimize the number of CSs based on the region where buses are closer to each other.

To obtain lower-bound expressions for the density of CSs that satisfies rejection and non-idle constraints, we start by obtaining the average number of EVs under each cluster, after which we present the charging price strategy. The obtained calculations are then used in the CSs queuing analysis that mimics the charging coordination mechanism, which then establishes the set of constraints for the dynamic program.

A. CALCULATING AVERAGE NUMBER OF EVs UNDER EACH CLUSTER

Let $\tau_c(t)$ be the area of cluster c region at time t. Each EV $z \in \Phi_{\text{EV}}(t)$ is associated with the nearest bus.

Definition 1: (Service region) The service region $\mathbb{A}_{b_j^{(c)}}(x_{b_j^{(c)}})$ in cluster c for each bus $b_j^{(c)}$ located at $x_{b_j^{(c)}} \in \Phi_{\text{B}}^{(c)}(t)$, where $\Phi_{\text{B}}^{(c)}(t) = \{\bigcup_{l\in\Phi_l} \Phi_{\text{B},l}(t)\} \cap \tau_c(t)$ forms a thinning HPPP from $\Phi_{\text{B}}(t)$ with density $\lambda_{\text{B}}^{(c)}(t)$, and it is defined as

$$\mathbb{A}_{b_j^{(c)}} = \left\{ z \in \mathbb{R}^2 : x_{b_j^{(c)}} = \underset{x_b \in \Phi_{\text{B}}^{(c)}(t)}{\text{argmin}} \|x_b - z\|_2 \right\}. \quad (2)$$

The service region of a bus contains all EVs that are the closest in distance to the bus, and therefore become served by the CSs accommodated by that bus.

The next step is to derive the average area of the service region at a typical bus. First, the area of the service region can be expressed as

$$|\mathbb{A}_{b_j^{(c)}}(x_{b_j^{(c)}})| = \int \prod_{x_b \in \Phi_{\text{B}}^{(c)}(t)} \mathbb{1}\left(\|x_{b_j^{(c)}} - z\|_2 < \|x_b - z\|_2 \right) dz. \quad (3)$$

Lemma 1: The average area of the service region can be expressed as

$$\mathbb{E}\left[|\mathbb{A}_{b_j^{(c)}}(x_{b_j^{(c)}})|\right] = \frac{1}{2\sqrt{\lambda_{\mathrm{B}}^{(c)}(t)}}. \tag{4}$$

Proof:

$$\begin{aligned}\mathbb{E}\left[|\mathbb{A}_{b_j^{(c)}}(x_{b_j^{(c)}})|\right] &\overset{(a)}{=} \mathbb{E}_{\Phi_{\mathrm{B}}^{(c)}(t)}\left[|\mathbb{A}_{b_j^{(c)}}(0)|\right] \\ &\overset{(b)}{=} \int_{\mathbb{R}^2} e^{-\lambda_{\mathrm{B}}^{(c)}(t)\int_{\mathbb{R}^2}\mathbb{1}(\|z\|_2\le\|x_b-z\|_2)dx_b}dz \\ &\overset{(c)}{=} \int_{\mathbb{R}^2} e^{-\lambda_{\mathrm{B}}^{(c)}(t)\pi\|z\|^2}dz = \frac{1}{2\sqrt{\lambda_{\mathrm{B}}^{(c)}(t)}},\end{aligned}$$

where (a) comes from assuming a typical bus at the origin using Slivniyaks theorem [27]; (b) uses the probability generating functional (PGFL) to evaluate the expectation over $\Phi_B^{(c)}(t)$ [27]; and (c) evaluates the integral in the exponential term as the area of a circle with radius $\|z\|$. This completes the proof. □

The average number of EVs under bus $b_j^{(c)}$ in cluster c

$$\mathbb{E}\left[N_{\mathrm{EV},b_j^{(c)}}\right] = \left(\lambda_{\mathrm{B}}^{(c)}(t)/\lambda_{\mathrm{EV}}^{(c)}(t)\right)\mathbb{E}\left[|\mathbb{A}_{b_j^{(c)}}|\right] \tag{5}$$

.

Theorem 1: The total average number of EVs under all buses in cluster c can be expressed as

$$\begin{aligned}\mathbb{E}\left[N_{\mathrm{EV}}^{(c)}\right] &= \sum_{j\in\Phi_{\mathrm{B}}^{(c)}}\mathbb{E}\left[N_{\mathrm{EV},b_j^{(c)}}\right] \\ &\overset{(a)}{=} \frac{\sqrt{\lambda_{\mathrm{B}}^{(c)}(t)}\sum_{l=1}^{\lambda_l\nu(c)}\lambda_{\mathrm{B},l}(t)|\ell_l^{(c)}|}{2\lambda_{\mathrm{EV}}^{(c)}(t)},\end{aligned} \tag{6}$$

where (a) comes from the fact that the number of Poisson lines intersecting the convex cluster region $c \subseteq \mathbb{R}^2$ follows a Poisson distribution with mean $\lambda_l\nu(c)$ where $\nu(c)$ is the perimeter of the convex cluster region c [28], and $|\ell_l^{(c)}|$ is the magnitude of line ℓ_l in cluster region c.

B. CHARGING PRICE STRATEGY

The pricing scheme adopted in this paper along with the queuing model described in Section III-C aim to model spatial and temporal coordination behavior of EV charging requests. Such a behavior maximizes the usage of deployed chargers by considering the possibility of spatial and temporal coordination of charging requests, which in turn minimizes the number of allocated chargers and EV CSs. This helps to prevent the over-provisioning of resources.

We consider that EVs' arrival follows a Poisson process with arrival rate $\lambda(t_{\mathrm{h}})$ at hour[2] $t_{\mathrm{h}} = \{1, \ldots, 24\}$ [29]–[32], and charging service time follows an exponential distribution with an average duration $\rho = 1/\mu$ [33]. Each EV selects one of the potential CSs $N_{\mathrm{CS}}^{(c)}(t)$ in cluster c as its desired CS based on charging price set by the system operator. Charging a flat price does not offer a solution to congestions when they occur. Since this is a long-term planning problem and it is not a real-time operational problem, only statistical measures are accounted for based on queuing theory. The pricing scheme adopted in this paper is similar in concept to the time-of-use (TOU) pricing scheme, where high electricity price is imposed at congestion times while lower tariff is used otherwise [34]. Hence, a normal price p_{norm} (same for all CSs) is offered when the arrival rate $\lambda(t_{\mathrm{h}})$ falls below a threshold $\lambda^*(t_{\mathrm{h}})$, and a congestion price $p_{\mathrm{cong}} > p_{\mathrm{normal}}$ is imposed when $\lambda(t_{\mathrm{h}}) > \lambda^*(t_{\mathrm{h}})$. The congestion price provides incentives for customers to move to less congested neighboring CSs in the cluster, which reflects a spatial coordination behavior. The threshold $\lambda^*(t_{\mathrm{h}})$ is related to the quality of service target $\delta_{\max}$, and is defined as [34]

$$\lambda^*(t_{\mathrm{h}}) = \begin{cases}\max \lambda(t_{\mathrm{h}}) \\ \text{s.t.} P_{\mathrm{BT}}(\lambda(t_{\mathrm{h}})) \le \delta_{\max},\end{cases}$$

where P_{BT} is the blocking probability to be defined in Section III-C. Using [34], the pricing $p(t_{\mathrm{h}})$ can be expressed as

$$p(t_{\mathrm{h}}) = \begin{cases} p_{\mathrm{norm}}, & \text{if } \lambda(t_{\mathrm{h}}) \le \lambda^*(t_{\mathrm{h}}) \\ p_{\mathrm{cong}} = p_{\mathrm{norm}}\left(1 + \theta_{\mathrm{p}}\sqrt{-\log\frac{\lambda^*(t_{\mathrm{h}})}{\lambda(t_{\mathrm{h}})}}\right), & \text{otherwise,}\end{cases}$$

where θ_p is a price tuning parameter set by operators to provide customers with incentives on where to charge EVs.

Each EV driver makes a charging decision based on pricing charge $p(t_{\mathrm{h}})$ at hour t_{h}, where he/she selects a CS s with selection probability $\beta(p(t_{\mathrm{h}}))$ represented by a diminishing and differentiable price sensitivity function [35], [36]:

$$\beta(p(t_{\mathrm{h}})) = \begin{cases} 1, & \text{if } \lambda(t_{\mathrm{h}}) \le \lambda^*(t_{\mathrm{h}}) \\ \max\left\{1 - \left(\frac{p(t_{\mathrm{h}})}{r_{\max}}\right)^2, 0\right\}, & \text{otherwise,}\end{cases} \tag{7}$$

$r_{\max}$ is the maximum charging price accepted by EV drivers.

C. QUEUING NETWORK ANALYSIS

The EVs charging system is composed of $N_{\mathrm{CS}}^{(c)}(t)$ CSs in cluster c, each having $g_{b_j^{(c)}} = \left\lfloor\left(L_{b_j^{(c)}} - P_{\mathrm{R}}(t)\right)/P_{\mathrm{c}}\right\rfloor$ maximum number of deployed chargers, where $L_{b_j^{(c)}}$ is the total load capacity of bus b_j in cluster c, $P_{\mathrm{R}}(t)$ is the regular load at time stage t, and P_{c} is the constant power drawn by each charger. We adopt the multi-server priority queue model, to capture the temporal charging coordination behavior, where each CS has two queues: one queue for incoming high-priority (HP) EVs that require charging at the current time slot (usually have smaller charging time); and one queue for low-priority (LP) EVs whose charging can be deferred to future slots.

[2]Note that t_{h} represents a scale of hours, which should not be confused with the notation t that represents a scale of years.

LP EVs can tolerate more delay than HP EVs to complete charging, and that is why LP EVs can be deferred to future available time slots. A real example would be an EV owner who is attending his/her work in an office, university or factory can be considered a low priority EV compared to a high priority EV such as an EV owner whose destination is a short stopover such as a shopping mall, a theatre, a restaurant, etc. Let $\lambda_{\mathrm{H}}(t_{\mathrm{h}})$ and $\lambda_{\mathrm{L}}(t_{\mathrm{h}})$ denote the arrival rates of HP EVs and LP EVs, respectively. Moreover, let $\rho_{\mathrm{H}}(t_{\mathrm{h}}) = \lambda_{\mathrm{H}}(t_{\mathrm{h}})/\mu_{\mathrm{H}}$ and $\rho_{\mathrm{L}}(t_{\mathrm{h}}) = \lambda_{\mathrm{L}}(t_{\mathrm{h}})/\mu_{\mathrm{L}}$ denote the average durations of the exponentially distributed charging service time for HP EVs and LP EVs, respectively. Given that EVs' arrival rates follow a Poisson process, and charging service times follow an exponential distribution, we can model the EVs charging system as a parallel $M/M/g/z$ queue, where $z_{b_j^{(c)}}$ is the size of CS at bus $b_j^{(c)}$, and $z_{b_j^{(c)}} = g_{b_j^{(c)}} + W_{\mathrm{HP}} + W_{\mathrm{LP}}$, with W_{HP} and W_{LP} representing the number of HP and LP EVs waiting to be charged, respectively [37], [38]. The queue is preemptive with a cut-off priority that operates as follows:

- LP EVs receive charging service only when the number of busy chargers $k < g'_{b_j^{(c)}}$, where $g'_{b_j^{(c)}}$ is a cut-off threshold for admitting LP EVs in the service [38].
- Once an LP EV is receiving service, we do not interrupt it if an HP EV arrives and all chargers are busy.
- HP EV receives charging service when the number of chargers $k < g_{b_j^{(c)}}$, i.e., there is at least one available charger; otherwise we place it in the HP waiting queue.
- All queued EVs (LP EVs and HP EVs) waiting to be charged are served in a first-come-first-serve (FCFS) order. Whenever a charger becomes available, an HP EV advances from its queue. LP EVs start to be charged when the HP queue is over.
- We reject an HP EV when $k = g_{b_j^{(c)}}$, i.e., all chargers are busy, and the HP queue if fully occupied.
- We reject an LP EV when $k \geq g'_{b_j^{(c)}}$ and there is not more available space in the LP waiting queue.

Then, HP EVs see an $M/M/g/z$ queue, while LP EVs access the $M/M/k/z$ queue ($k < g'_{b_j^{(c)}}$).

The above queuing process can be modeled as a two-dimensional Markov chain for each CS with the state transition diagram consisting of states of the number of HP and LP EVs, and the transitioning occurs when new HP and LP EVs arrive at the system or depart the system (see Fig.5 in [38]). Let $\pi\,(N_{\mathrm{H}}, N_{\mathrm{L}}, k)$ be the steady-state probability of the system, where N_{H} and N_{L} denote the number of queued HP EVs and LP EVs, respectively; and k is the number of plug-in busy chargers. For notation simplicity, we drop t_{h} and we use g instead of $g_{b_j^{(c)}}$. Furthermore, let π_k^{cut} be the steady-state probability taking the cut-off priority threshold into consideration, and defined in [38] as

$$\pi_k^{\mathrm{cut}} = \begin{cases} \pi_0^{\mathrm{cut}} \rho^k / k!, & 0 \leq k \leq g' \\ \pi_0^{\mathrm{cut}} \left(\rho^{g'} \rho_{\mathrm{H}}^{k-g'} / k! \right) g' / \left(g' - \rho_{\mathrm{L}} T(g', g) \right), & \\ \qquad g' \leq k \leq g-1 \\ \pi_0^{\mathrm{cut}} \left(\rho^{g'} \rho_{\mathrm{H}}^{k-g'} / g! \right) \left[g' / \left(g' - \rho_{\mathrm{L}} T(g', g) \right) \right] g / \left(g - \rho_{\mathrm{H}} \right), & \\ \qquad k = g, \end{cases}$$

where $\rho = \rho_{\mathrm{H}} + \rho_{\mathrm{L}}$; and

$$\pi_0^{\mathrm{cut}} = \left[\sum_{i=0}^{g'-1} \rho_i / i! + \frac{\left(\rho^{g'} / \left(g'-1 \right)! \right) T(g', g)}{\left(g' - \rho_{\mathrm{L}} T(g', g) \right)} \right]^{-1}$$

$$\text{and } T(g', g) = \rho_{\mathrm{H}}^{-g'} g'! \left(\sum_{i=g'}^{g-1} \rho_{\mathrm{H}}^{-i} / i! + \left(\rho_{\mathrm{H}}^{g} / g! \right) g / \left(g - \rho_{\mathrm{H}} \right) \right).$$

The blocking probability is given by $P_{\mathrm{BT}}(\lambda(t_{\mathrm{h}})) = \pi_g^{\mathrm{cut}}$.

Let $p_{s,s}\,(p(t_{\mathrm{h}})) = \beta\,(p(t_{\mathrm{h}}))$ denote the probability that an EV access a CS s to get charged. Variable $\beta(p(t_{\mathrm{h}}))$ is defined in Eq. (7). Furthermore, let $p_{s,s'}\,(p(t_{\mathrm{h}})) = (1 - \beta\,(p(t_{\mathrm{h}})))\,\alpha_{s'|s}$ denote the probability that an EV routes to CS s' from CS s, where $\alpha_{s'|s}$ is the probability that an EV visits CS s' after visiting CS s [35].

We introduce the binary variable $x_v \in \{0, 1\}$ to capture the charging need of EV v:

$$x_v = \begin{cases} 1, & \text{if EV } v \text{ requires charging} \\ 0, & \text{otherwise.} \end{cases}$$

Using the above notations, probabilities, and Theorem 1, we can express the average number of busy chargers at CS s accommodated by bus $b_j^{(c)}$ in cluster c as

$$B_s^{(c)}\,(N_{\mathrm{H}}, N_{\mathrm{L}}, k(s)) = p_{s,s}\,(p_{\mathrm{norm}})\,\pi\,(0, 0, g(s))\,\varrho, \tag{8}$$

for $1 \leq k(s) \leq g(s)$, where $\pi\,(0, 0, g(s)) = (\rho^{g}(s)/g(s)!)\,\pi_0^{\mathrm{cut}}$ [38]; $k(s)$ is the number of busy plug-in chargers for CS s; $g(s)$ is the maximum number of busy plug-in chargers for CS s; and $\varrho = \sum_{v \in \mathbb{V}_{\mathbb{b}_{\mathbb{j}}^{(c)}}(t)} x_v\, \mathbb{E}\left[N_{\mathrm{EV}, b_j^{(c)}} \right] \rho$; $\mathbb{V}_{\mathbb{b}_{\mathbb{j}}^{(c)}}(t) = \{1, \ldots V_{b_j^{(c)}}(t)\}$ is the set of EVs at bus $b_j^{(c)}$ at a given time slot. Note that each CS can present a different number of deployed chargers due to the varying load capacities at buses.

The average number of queued EVs waiting to be charged at CS s accommodated by bus $b_j^{(c)}$ for $g'(s) \leq k(s) \leq g(s)$:

$$Q_s^{(c)}\,(N_{\mathrm{H}}, N_{\mathrm{L}}, k(s)) = p_{s,s}\left(p_{\mathrm{cong}}\right) \pi_{k(s)}^{\mathrm{cut}} \varrho. \tag{9}$$

The average number of routed EVs at CS s accommodated by bus $b_j^{(c)}$ in cluster c can be expressed as

$$R_s^{(c)}\,(N_{\mathrm{H}}, N_{\mathrm{L}}, k(s)) = p_{s,s'}\,(p(t))\,\frac{\varrho}{\rho}\left(\pi_{k(s)}^{\mathrm{cut}} \rho_{\mathrm{L}} + \pi_{g(s)}^{\mathrm{cut}} \rho_{\mathrm{H}} \right), \tag{10}$$

for $g'(s) \leq k(s) \leq g(s)$.

Thus, the average number of rejected EVs at CS s accommodated by bus $b_j^{(c)}$ in cluster c can be expressed as

$$D_s^{(c)}\left(N_{\mathrm{H}}, N_{\mathrm{L}}, k(s)\right) = \varrho - R_s^{(c)} - \left(B_s^{(c)} + Q_s^{(c)}\right). \quad (11)$$

Let $\delta^{(c)}(t)$ be the density of CSs in cluster c at time stage t. It can be expressed as $\delta^{(c)}(t) = N_{\mathrm{CS}}^{(c)}(t) \sum_{b_j^{(c)} \in \Phi_{\mathrm{B}}^{(c)}(t)} g_{b_j^{(c)}} / \tau_c(t)$.

Lemma 2: Let γ_{r} be the threshold of rejected EVs, then a lower-bound expression on $\delta^{(c)}(t)$ can be obtained as follows:

$$\delta^{(c)}(t)\tau_c(t) \sum_{b_j^{(c)} \in \Phi_{\mathrm{B}}^{(c)}(t)} g_{b_j^{(c)}} D_{s,\mathrm{avg}}^{(c)}\left(N_{\mathrm{H}}, N_{\mathrm{L}}, k(s)\right) < \gamma_r$$

$$\Rightarrow \delta^{(c)}(t) \geq \frac{2\gamma_{\mathrm{r}}\lambda_{\mathrm{EV}}^{(c)}(t)}{\tau_c(t) \sum_{b_j^{(c)} \in \Phi_{\mathrm{B}}^{(c)}(t)} g_{b_j^{(c)}} \sqrt{\lambda_{\mathrm{B}}^{(c)}(t)} \Upsilon_{\mathrm{a}} \sum_{v \in \mathbb{V}_{\mathbb{b}_{\mathbb{j}}^{(c)}}(t)} x_v},$$

where

$$\Upsilon_{\mathrm{a}} = \left(1 - \frac{1}{\rho} p_{s,s'}\left(p(t)\right)\left(\pi_{k(s),\mathrm{avg}}^{\mathrm{cut}} \rho_{\mathrm{L}} + \pi_{g(s),\mathrm{avg}}^{\mathrm{cut}} \rho_{\mathrm{H}}\right)\right) - p_{s,s}\left(p_{\mathrm{norm}}\right) \pi_{\mathrm{avg}}\left(0, 0, g(s)\right) - p_{s,s}\left(p_{\mathrm{cong}}\right) \pi_{k(s),\mathrm{avg}}^{\mathrm{cut}}, \text{ and} \quad (12)$$

π_{avg} is the average probability over all CSs.

Lemma 3: Similarly, let γ_{d} be the non-idle threshold, then a lower-bound expression on $\delta^{(c)}(t)$ can be obtained as

$$\delta^{(c)}(t)\tau_c(t) \sum_{b_j^{(c)} \in \Phi_{\mathrm{B}}^{(c)}(t)} g_{b_j^{(c)}} B_{s,\mathrm{avg}}^{(c)}\left(N_{\mathrm{H}}, N_{\mathrm{L}}, k(s)\right) \geq \gamma_{\mathrm{d}}$$

$$\Rightarrow \delta^{(c)}(t) \geq \frac{2\gamma_{\mathrm{d}}\lambda_{\mathrm{EV}}^{(c)}(t)}{\tau_c(t) \sum_{b_j^{(c)} \in \Phi_{\mathrm{B}}^{(c)}(t)} g_{b_j^{(c)}} \rho \sqrt{\lambda_{\mathrm{B}}^{(c)}(t)} \Upsilon_{\mathrm{b}}}, \quad (13)$$

where $\Upsilon_{\mathrm{b}} = p_{s,s}\left(p_{\mathrm{norm}}\right) \pi_{\mathrm{avg}}\left(0, 0, g(s)\right) \sum_{v \in \mathbb{V}_{\mathbb{b}_{\mathbb{j}}^{(c)}}(t)} x_v$.

Theorem 2: The resulting lower-bound expression for the CSs density in cluster c at time stage t such that the rejection (γ_{r}) and the non-idle charging thresholds (γ_{d}) are satisfied is

$$\delta^{(c)}(t) \geq \max\left\{\text{Eq.(12), Eq.(13)}\right\}. \quad (14)$$

Proof: It follows from taking the maximum of the lower-bound expressions on $\delta^{(c)}(t)$ from Lemma 2 and 3. □

D. IMPACT FACTORS OF BUSES

In this subsection, we describe the process of calculating the impact factors of buses in terms of the size of CSs and the density of EVs in order to determine where to install CSs. When we obtain at each time stage the number of CSs and DG units to be allocated, we need to specify their locations. This is where the impact factor criteria comes into play. A bus with a large load capacity is capable of accommodating multiple CSs. That bus becomes important as the CSs it accommodates will be able to serve a larger number of EVs. Similarly, the EV density associated with a particular bus dictates the importance of that bus, since the CSs hosted by that bus are expected to serve as many EVs as possible.

We calculate the impact factor of each bus based on two criteria: i) the CS size determined by the maximum number of chargers, $g_{b_j^{(c)}}$, that a bus $b_j^{(c)}$ can support, and ii) the EVs density associated with that bus. We obtain the EVs density $\lambda_{\mathrm{EV},b_j^{(c)}}$ by associating EVs to buses that are the closest to them based on distances between them.

Finally, we calculate the impact factor of bus $b_j^{(c)}$ as

$$\mathrm{IF}_{b_j^{(c)}} = w_{\mathrm{CS}} g_{b_j^{(c)}} + w_{\mathrm{EV}} \lambda_{\mathrm{EV},b_j^{(c)}}, \quad (15)$$

where w_{CS} and w_{EV} are weight factors associated with CSs size and EV density, respectively; and $w_{\mathrm{CS}} + w_{\mathrm{EV}} = 1$. Once the number of CSs in each cluster at each time stage is determined by the constraints of Theorem 2, CSs shall first be deployed at buses with the highest impact factors.

IV. FINITE-HORIZON DYNAMIC PROGRAMMING MODEL

In this section, we present the multi-year planning dynamic problem, whose solution allows system operators to determine the number and locations of CSs and DGs in each year that minimize costs given a budgetary limit and rejection and non-idle constraints. This section is organized as follows:

- We start by describing the joint allocation problem of CSs and DGs in the context of dynamic programming based on the principle of optimality [39] in Subsection IV-A, where we define a decision variable vector ϑ_t, a state variable vector s_t, a transition function f_t, and a cost function c_t, corresponding to each stage t.
- In Subsection IV-B, we formulate the linear dynamic program given the cost function and state variables defined in Section IV-A.
- In Section IV-C, we introduce the algorithms that solve the optimization problem described in Section IV-B and we explain how they find the optimal solution.
- Subsection IV-D discusses the computational complexity of the algorithms and the effect of the number of clusters and the density of EVs and buses on the scalability of the proposed solution.

A. STATE VARIABLES AND CONTROL ACTIONS

In this subsection, we describe the state decision variables, transition and cost functions that set up the dynamic programming allocation of CSs and DGs in each cluster.

The decision variable at time t captured by vector $\vartheta_t = \{n_{\mathrm{CS},t}^{(c)}, x_{\mathrm{CS},t}^{(c)}, n_{\mathrm{DG},t}^{(c)}\}$ is a tuple consisting of the number of CSs to allocate, their corresponding locations and the number of DG units to install at t in cluster c. The state variable at time t, represented by vector $s_t = \{m_t^{(c)}, \chi_t\}$, is a tuple consisting of the number of already allocated CSs in the grid until t in cluster c, $m_t^{(c)}$, and the state of the budget at t, χ_t. The transition function, f_t, is defined by the Poisson PMF since the number of new buses and the number of new EVs added at each time stage are Poisson random variables:

$f_t = \left(\lambda_{\mathrm{B}}^{n_{\mathrm{b},t}} \lambda_{\mathrm{EV}}^{n_{\mathrm{EV},t}}\right) e^{-(\lambda_{\mathrm{B}}+\lambda_{\mathrm{EV}})} / \left(n_{\mathrm{b},t}! n_{\mathrm{EV},t}!\right)$, where $n_{\mathrm{b},t}$ and $n_{\mathrm{EV},t}$ are the number of buses and the number of EVs added at time stage t, respectively.

Let a represent the fixed installation cost of a single electric charger. Then, a single CS's installation cost at bus location $x_{b,t}^{(c)}$ is given by $q_{\mathrm{c},x_b(t)^{(c)}} = a g_{x_{b,t}^{(c)}}$. Assuming the cost of a DG unit, q_{DG}, equals the sum of the capital cost and operation costs, the cost function $c_t(s_t, \vartheta_t)$ for $t \in \{1, \ldots, T\}$ is expressed as

$$c_t(s_t, \vartheta_t)^{(c)} = \sum_{x_b \in x_{\mathrm{CS},t}^{(c)}} q_{\mathrm{c},x_b(t)^{(c)}} + q_{\mathrm{DG}} n_{\mathrm{DG},t}^{(c)}. \tag{16}$$

B. OPTIMIZATION PROBLEM FORMULATION

We now formulate a linear dynamic program whose objective is to minimize the overall deployment cost over T stages:

$$\underset{n_{\mathrm{CS},t}, n_{\mathrm{DG},t}}{\text{minimize}} \sum_{c \in \mathcal{C}} \sum_{\mathcal{T}} c_t(s_t, \vartheta_t)^{(c)} \tag{17}$$

$$\text{subject to } \delta^{(c)}(t) \geq \max\{\text{Eq.(12), Eq.(13)}\}, \ \forall c \in \mathcal{C}, \tag{18}$$

$$L'_{b_j^{(c)}} > 0, \ \text{if } N_{\mathrm{CS},b_j}^{(c)}(t) > 1, \ b_j^{(c)} \in \Phi_{\mathrm{B}}^{(c)}(t), c \in \mathcal{C} \tag{19}$$

$$0 < \chi_t \leq \chi_{\mathrm{tot}}, \tag{20}$$

$$n_{\mathrm{CS},t}^{(c)}, n_{\mathrm{DG},t}^{(c)} \geq 0, \quad \forall c \in \mathcal{C}, \tag{21}$$

where constraint (18) ensures that the density of CSs in each cluster satisfies the rejection and non-idle constraints obtained in Theorem 2; constraint (19) ensures that there is an additional load $L'_{b_j^{(c)}}$ required by bus b_j in cluster c if there are at least two or more CSs that can be allocated at that bus; constraint (20) ensures that the remaining budget at time t does not exceed the total pre-allocated budget χ_{tot}; and constraint (21) captures the non-negativity of the number of CSs and DGs to allocate.

The state space at t in cluster c is $s(t)^{(c)} \in \{m_t, \chi_t\}$. Associated with this state is the amount of rejection and non-idle amount of EVs $\gamma_{\mathrm{r},t}, \gamma_{\mathrm{d},t}$, respectively, in the same time stage t. The states are related in a causal and sequential manner, i.e., s_t—s_{t-1}—s^{t-2} forms a Markov chain for all t, where s^{t-2} denotes the collection of the past $t-2$ states [40][3]. Hence, the optimization in (17)-(21) represents a finite-horizon constrained Markov decision process (MDP).

For each pair of the threshold constraints $\epsilon_t = \{\gamma_{\mathrm{r},t}, \gamma_{\mathrm{d},t}\}$, we calculate the minimum number of CSs and DGs required to satisfy ϵ_t. Then, we allocate the CSs in each cluster by installing them on buses starting with the node with the highest impact factor $\mathrm{IF}_{b_j^{(c)}}$ first, as given in (15).

C. SOLVING THE CONSTRAINED FINITE-HORIZON MDP

Algorithm 2 attempts to solve the constrained MDP described in (17)-(21) by finding the optimal number of CSs to install in each year in order to satisfy the total budget constraint. Algorithm 2 takes as input the time axis $\mathcal{T} = \{1, \ldots, T\}$; the state space S; the state transition matrix P; a set of control actions $\Phi(s_t)$, and outputs the optimal control policies $\mathcal{M} = \{\mu_1, \mu_2, \ldots \mu_T\}$ at each stage by solving the dynamic programming backward in time from stage T up to stage 1 [41], [42]. For each time step and for each pair of charging constraints, Algorithm 2 calls the CSs and DGs allocation functions definitions at lines 5 and 6. These functions definitions are introduced in Algorithm 3. The CSs and DGs allocation functions ('allocateCS' and 'calcDG') provide the search space of the number of CSs and DGs that need to be allocated on each bus at each time stage to satisfy the charging service constraints, but not the budgetary limit.

After the search space is obtained, we calculate the reward function at line 9. The reward function at bus $b_j^{(c)}$ is determined by the total number of CSs, $n_{b_j,t}^{(c)}$, to allocate at that bus, as determined by the function 'allocateCS'. Then, the search space consists of the total number of CSs to allocate on all buses in all clusters, for each control action specified by a rejection and a non-idle charging constraint threshold. For each reward obtained, we calculate at line 11 the total cost of installing the total number of CSs and DG units in all buses in all clusters. Then, at line 12, the achieved control actions are obtained when the total cost exceeds χ_{tot}.

Lines 16-19 finds an optimal solution to the objective function in Eq. (17) by solving the dynamic program backward in time, where at each stage t, the total reward is minimized over all control policies such that the budget constraint, χ_{total}, is satisfied, i.e. satisfying Eq. (20). The optimal control policy μ_t^* is the one achieving the minimum reward.

Algorithm 3 specifies two function definitions that are called within Algorithm 2. The first function is 'allocateCS', which allocates the total number of CSs, $n_{\mathrm{CS},t}^{(c)}$, for each bus to satisfy certain rejection and non-idle charging thresholds. The value of $n_{\mathrm{CS},t}^{(c)}$ is obtained by Eq.(18). This allocation satisfies only the technical charging constraints, $\gamma_{\mathrm{r},t}$ and $\gamma_{\mathrm{d},t}$, but not the total budgetary constraint, χ_{total}. Therefore, 'allocateCS' attempts to find a search space of CSs that will need to be optimized by lines 16-19 of Algorithm 2 to satisfy the budget constraint over all years of deployment.

The function 'allocateCS' starts by finding the bus with the highest impact factor as described by Section III-D (line 5) and allocates a single CS (line 6), then finds the bus with the second highest impact factor and allocates a CS, and so on until all CSs specified by $n_{\mathrm{CS},t}^{(c)}$ have been allocated (lines 9-11) or all buses have already been visited (lines 4 and 8). In the case where all buses have a single CS allocated to each one of them and there is still a number of CSs to allocate (line 14), then we find again the bus with the highest impact factor (line 18) and we allocate a single CS (line 19). This process continues until all $n_{\mathrm{CS},t}^{(c)}$ have been allocated (lines 22-24).

[3]The subscript notation refers to the current time stage only, and the superscript refers to the collection of all time stages up to the current stage.

Algorithm 2 Solving the Constrained Finite-Horizon MDP

Input: $\mathcal{T} = \{1, \ldots, T\}$; a state space S; a state transition matrix P; a set of control actions $\mathbb{O}(s_t)$; the set of buses $\{B^{(c)}\}$ in c; the impact factors $\{\text{IF}^{(c)}\} = \{\text{IF}_{b_j^{(c)}} | b_j^{(c)} \in \{B^{(c)}\}\}$ in c; the set of load capacities $\{L^{(c)}\} = \{L_{b_j^{(c)}} | b_j^{(c)} \in \{B^{(c)}\}\}$; $n_{\text{CS},t}^{(c)}$; and $P_{\text{R}}(t)$

Output: Optimal control policies $\mathcal{M} = \{\mu_1, \mu_2, \ldots \mu_T\}$

1: **begin**
2: **for** $t = 1 \ldots T$ **do**
3: **foreach** $\epsilon_t = \{\gamma_{\text{r},t}, \gamma_{\text{d},t}\}$ **do**
4: **foreach** $c \in |C|$ **do**
5: $\{n_{b_j,t}^{(c)}\} \leftarrow$ ALLOCATECS($\{B^{(c)}\}$, $\{\text{IF}^{(c)}\}$, ϵ_t, $n_{\text{CS},t}^{(c)}$)
6: $\{L^{(c)'}\} \leftarrow$ CALC(DG$\{B^{(c)}\}$, $\{n_{b_j,t}^{(c)}\}$, $\{L^{(c)}\}$, $P_{\text{R}}(t)$)
7: **end for**
8: **foreach** control action $o(s_t) \in \mathbb{O}(s_t)$ **do**
9: Define immediate reward function $r_t = \{\sum_{c\in\mathcal{C}} \sum_{b_j^{(c)}\in\{B^{(c)}\}} n_{b_j,t}^{(c)}(s, o, \epsilon) : s \in S_t, o \in \mathbb{O}(s_t)\}$
10: Reward obtained: $R_t = r_t(s_t, o_t, \epsilon)$
11: Calculate total cost TC_t corresponding to the number of allocated CSs and DG units as $\text{TC}_t(R_t) = q_c R_t + q_{\text{DG}} \sum_{c\in\mathcal{C}} \sum_{b_j^{(c)}\in\{B^{(c)}\}} L'_{b_j^{(c)}}$
12: Obtain the set of control actions $\mathbb{O}'(s_t) = \{\mathbb{O}(s_t) : \sum_{k=1}^{t} \text{TC}_k(R_k) \leq \chi_{\text{tot}}\}$
13: **end for**
14: **end for**
15: **end for**
16: Define the optimal value function at stage T as $V_T^*(s) = r_T(s)$
17: Compute the value function $V_k^{\mu}(s)$ by backward recursion [43], for $k = \{T, \ldots, 1\}$:

$$V_k^{\mu}(s_k) = \{R_k + \sum_{s'\in S_{k+1}} p_k(s'|s_k, o_k) V_{k+1}^{\mu}(s')\}_{o_k=\mu_k(s_k)}$$

18: Starting with $V_T^*(s)$, obtain the optimal value function:

$$V_k^*(s_k) = \min_{o_k\in\mathbb{O}'(s_k)} \{R_k + \sum_{s'\in S_{k+1}} p_k(s'|s_k, o_k) V_{k+1}^*(s')\}$$

19: The optimal control policy μ^* satisfies

$$\mu_k^*(s_k) \in \underset{o_k\in\mathbb{O}'(s_k)}{arg\,min} \{R_k + \sum_{s'\in S_{k+1}} p_k(s'|s_k, o_k) V_{k+1}^*(s')\}$$

20: **end**

Algorithm 3 Definitions of CSs and DGs Allocation Functions

1: **function** allocateCS($\{B^{(c)}\}$, $\{\text{IF}^{(c)}\}$, ϵ_t, $n_{\text{CS},t}^{(c)}$): $\{n_{b_j,t}^{(c)}\}$
2: ▷ *This function allocates $n_{b_j,t}^{(c)}$ CSs for each bus $b_j^{(c)}$*
3: count$\leftarrow 0$
4: **while** $\{B^{(c)}\} \neq \emptyset$ **do**
5: Find bus $b_j^{(c)}$ with highest $\text{IF}_{b_j^{(c)}}$
6: Allocate a single CS on $b_j^{(c)}$: $n_{b_j,t}^{(c)} \leftarrow 1$
7: count$\leftarrow$ count+1
8: $\{B^{(c)}\} \setminus b_j^{(c)}$
9: **if** count$== n_{\text{CS},t}^{(c)}$ **then**
10: Break
11: **end if**
12: **end while**
13: $\{B^{(c)}\} = \{b_j^{(c)} | x_{b_j^{(c)}} \in \Phi_B^{(c)}\}$
14: **while** count$< n_{\text{CS},t}^{(c)}$ **do**
15: **if** $\{B^{(c)}\} == \emptyset$ **then**
16: $\{B^{(c)}\} = \{b_j^{(c)} | x_{b_j^{(c)}} \in \Phi_B^{(c)}\}$
17: **end if**
18: Find bus $b_j^{(c)}$ with highest $\text{IF}_{b_j^{(c)}}$
19: Allocate CS on $b_j^{(c)}$: $n_{b_j,t}^{(c)} \leftarrow n_{b_j,t}^{(c)} + 1$
20: count$\leftarrow$ count+1
21: $\{B^{(c)}\} \setminus b_j^{(c)}$
22: **if** count$== n_{\text{CS},t}^{(c)}$ **then** Break
23: **end if**
24: **end while**
25: **end function**
26:
27: **function** CALCDG($\{B^{(c)}\}$, $\{n_{b_j,t}^{(c)}\}$, $\{L^{(c)}\}$, $P_{\text{R}}(t)$): $\{n_{\text{DG},b_j^{(c)},t}^{(c)}\}$, $\{L^{(c)'}\}$
28: ▷ *This function allocates DGs for each bus*
29: **while** $\{B^{(c)}\} \neq \emptyset$ **do**
30: DG units to install on $b_j^{(c)}$: $n_{\text{DG},b_j^{(c)},t}^{(c)} \leftarrow n_{b_j,t}^{(c)} - 1$
31: Additional load capacity required at bus $b_j^{(c)}$: $L'_{b_j^{(c)}} \leftarrow \lfloor L_{b_j^{(c)}} - P_{\text{R}}(t) \rfloor n_{\text{DG},b_j^{(c)},t}^{(c)}$
32: $\{B^{(c)}\} \setminus b_j^{(c)}$
33: **end while**
34: **end function**

In order to compensate for the expected increment in the load due to the dynamic installation of such EV CSs, we present function 'calcDG' in Algorithm 3, where the number of DG units to install at each stage t on each bus is calculated as the number of CSs that get allocated to the bus minus 1 (line 30), since initially the buses that can accommodate a single CS are selected from the set of all buses in the cluster. This means that any additional CS that has been allocated by lines 14-24 in function 'allocateCS', will accrue additional load capacity that is calculated by line 31. Line 31 satisfies the constraint in Eq. (19). The buses with small load capacities are not selected as candidates for CSs allocation.

In the case of CSs being initially installed in the power grid, then the dynamic program of Algorithm 2 can be run without additional changes. Then, after obtaining the CSs allocation

TABLE 2. Simulation parameters for validating the stochastic geometry power grid model.

Radius of the geographical region: $R = 232$ km
Number of Poisson lines: Poiss(20)
Number of buses on each Poisson line: Poiss($\lambda_{b,l}$) $= 6$
Nearest neighbors $k_i = [1, 2, 3, 4]$ with probabilities $\eta_i = [0.3252, 0.39837, 0.21951, 0.04065]$
$T = 1$ (no temporal expansion)

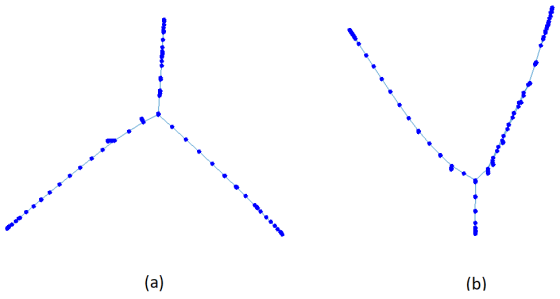

FIGURE 2. Graph tree structures of (a) the stochastic geometry model of Fig. 1, and (b) the IEEE 123-bus system.

solution, the obtained number of CSs can be subtracted from the already installed ones.

D. ON THE COMPUTATIONAL COMPLEXITY

For a fixed pre-determined number of clusters, $|C|$, and pre-determined bus and EV densities, λ_{B} and λ_{EV}, respectively, the computational complexity of Algorithm 2 is $\mathcal{O}(T \cdot |\epsilon_t|)$, where $|.|$ is the cardinality set. As the total number of electrical buses, and the number of EVs in the region increase, the computational complexity of Algorithm 2 increases linearly.

As for the effect of increasing the number of clusters, the computational complexity of Algorithm 2 scales linearly with the number of clusters $|C|$. For each cluster, Algorithm 3 is run to obtain the search space of the allocated number of CSs and DGs, which is then summed over all clusters at line 9 in Algorithm 2 to calculate the corresponding reward function. Thus, only the computational complexity of Algorithm 2 increases linearly as $\mathcal{O}(T \cdot |\epsilon_t| \cdot |C|)$, with the increase in number of clusters.

V. SIMULATION RESULTS AND ANALYSIS

A. VALIDATION OF THE STOCHASTIC-GEOMETRY POWER GRID MODEL

In this section, we validate our proposed power grid model by comparing it to the IEEE 123-bus system in terms of bus degree distribution, node betweenness centrality, eigenvalues spread and power grid diameter. For comparison purpose, we use the MATLAB library 'MatlabBGL' provided by [44], and the simulation parameters of Table 2.

Fig. 2 shows the topological graph tree structures of both the IEEE 123-bus system and the stochastic model of Fig. 1.

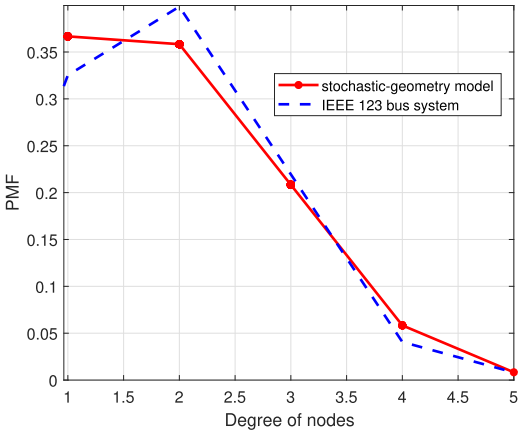

FIGURE 3. Comparison between the IEEE 123-bus system and the stochastic geometry-based model in terms of bus degree distribution.

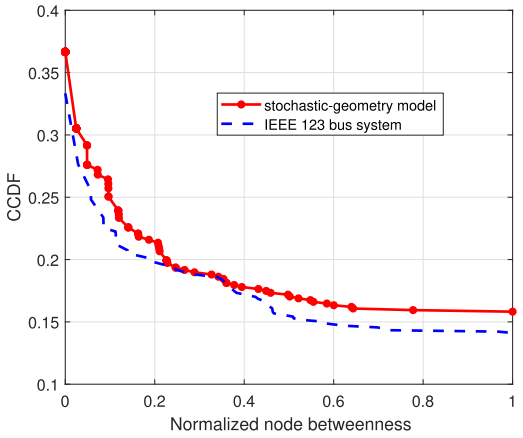

FIGURE 4. Comparison of node betweenness centrality for IEEE 123-bus system and the stochastic geometry-based model.

1) BUS DEGREE DISTRIBUTION

Fig. 3 shows the PMF of the average bus degree distribution of the stochastic geometry-based power grid model and that of IEEE 123-bus system. A similarity between both power grids can be depicted from Fig. 3, where the node degree distributions exhibits a right-skewed shape. This justifies the use of shifted sum of exponential distributions as an accurate approximation to real power grids [6].

2) NODE BETWEENNESS CENTRALITY

The node betweenness centrality provides information on the extent to which a bus is important in terms of power flow. A high bus betweenness centrality score indicates that a large number of buses passes through its path [45]. A plot of the complementary cumulative distribution function (CCDF) of node betweenness centrality in Fig. 4 reveals a resemblance between the stochastic geometry-based power grid model and that of IEEE 123-bus system.

3) POWER GRID DIAMETER

This metric represents the longest path that connects a pair of bus nodes among all the paths connecting any pair of bus

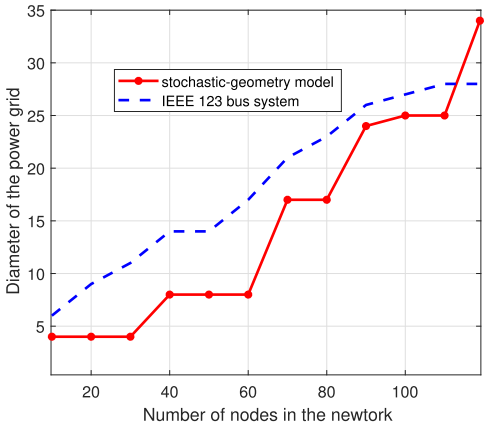

FIGURE 5. Comparison between the IEEE 123-bus system and the stochastic geometry-based model in terms of power grid's diameter.

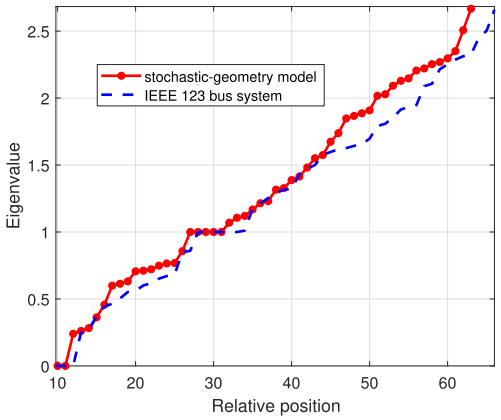

FIGURE 6. Comparison of spread of eigenvalues between the IEEE 123-bus system and the stochastic geometry-based model.

TABLE 3. Simulation parameters.

Average number of EVs: Poiss(5)
Number of buses $n_{b,t}$ added at $t > 1$: $n_{b,t} \sim$ Poiss(6)
Average number of EVs $n_{\mathrm{EV},t}$ added at $t > 1$: $n_{\mathrm{EV},t} \sim$ Poiss(30)
Number of clusters: $\lvert\mathcal{C}\rvert = 3$
Weight factors associated with CSs size and EV density, respectively: $w_{\mathrm{CS}} = 0.4$ and $w_{\mathrm{EV}} = 0.6$
Regular load $P_{\mathrm{R}} = 10$ kWh and power of each charger is $P_{\mathrm{c}} = 4.8$ kWh
Arrival rate: $\lambda_{\mathrm{H}}(t_{\mathrm{h}}) = \lambda_{\mathrm{L}}(t_{\mathrm{h}}) = 8 + \left(N_{\mathrm{EV}}^{(c)}/30\right) \sin(2\pi t_{\mathrm{h}}/80)$ [34]; and $\mu_{\mathrm{H}} = \mu_{\mathrm{L}} = 10$
Price tuning parameter $\theta_{\mathrm{p}} = 0.5$
Probability of EV visiting CS s': $\alpha_{s'\lvert s} = 0.5$
Charging socket installation cost $a =$ \$250 [47]
DG unit cost $q_{\mathrm{DG}} =$ \$1104.032/kWh [48]
Rejection threshold $\gamma_{\mathrm{r}} = 0.1$; and non-idle threshold $\gamma_{\mathrm{d}} = 0.9$

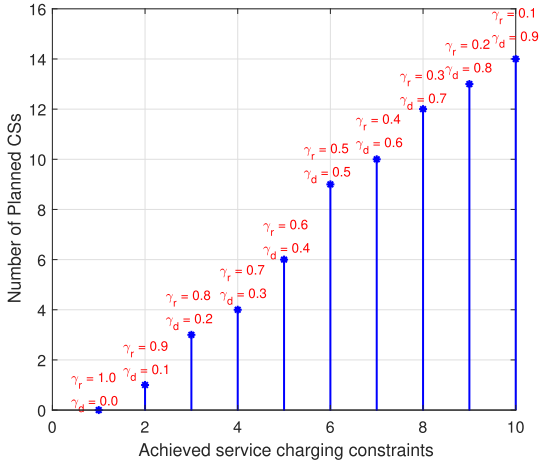

FIGURE 7. Minimum number of CSs to install to achieve different service charging constraints.

nodes in the whole grid. Because our model connects buses based on their physical boundaries and paths, we can accurately capture this topological metric. From Fig. 5, we see a similarity in performance between the stochastic geometry-based power grid model and that of IEEE 123-bus system.

4) EIGENVALUES SPREAD

The eigenvalues spread measures the extent to which a graph is connected. Fig. 6 reveals a comparable performance between our model and that of IEEE 123-bus system.

Simulation results revealed an average similarity score of 96.66%, with 98.86% for the betweenness centrality, 96.12% for the bus degree distribution, 99.14% for the eigenvalues spread, and 92.53% for power grid diameter. Given a certain realization of the developed stochastic geometry-based power grid model as input with spatial correlation of buses and lines, Algorithm 2 can then be applied to obtain the optimal spatial locations and installation time of EV CSs and DGs, while taking into consideration the geographical pattern and constraints of the region under study.

B. MULTI-YEAR JOINT ALLOCATION OF EVS AND DGS

In this section, we demonstrate a case study using the model of Fig. 1 for the multi-year CSs allocation problem over a period of 5 years, with the initial assumption that CSs have not been previously allocated. It should be noted that existing CSs allocation algorithms, mentioned in Section I-C, do not account for spatio-temporal expansion of the power grid and EVs, and therefore it is difficult to compare them to our proposed allocation strategy. To generate the results, we use the MDPtoolbox functions in MATLAB provided by [46]. Since our paper is mainly concerned about EV CSs planning, we then consider that regular electric loads are fixed throughout the years. Table 3 summarizes the parameters used.

First without considering any spatio-temporal expansion, we study the effect of EVs and charging constraints on the minimum number of CSs to be installed. Fig. 7 shows the minimum number of CSs to install to achieve different values of rejection and non-idle constraints. We can see that 14 CSs, each having $\sum_{j\in\Phi_b^{(c)}} g_{b_j^{(c)}}$ maximum number of deployed chargers, need to be installed in order to achieve the target charging constraints: $\gamma_{\mathrm{r}} = 0.1$ and $\gamma_{\mathrm{d}} = 0.9$. As these constraints get relaxed, less number of CSs will be needed.

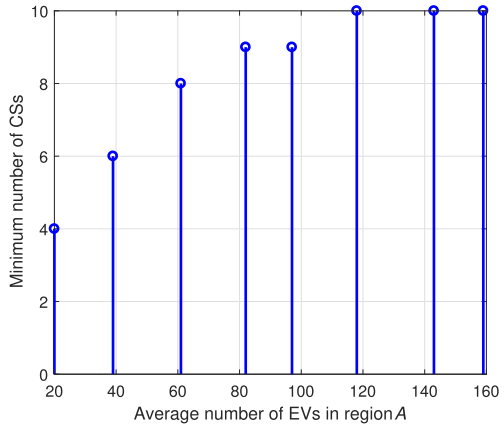

FIGURE 8. Minimum number of CSs to install to achieve $\gamma_d = 0.9$ and $\gamma_r = 0.1$ versus the total number of EVs in region $\mathcal{A}$.

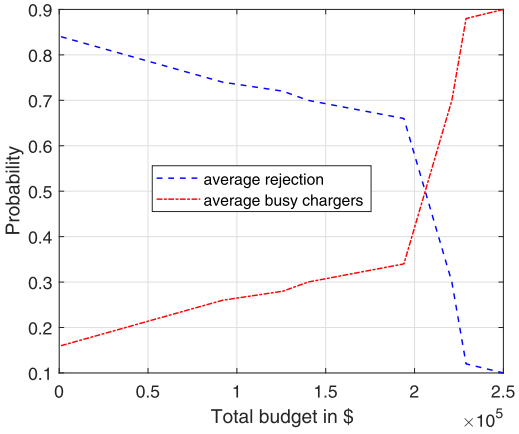

FIGURE 9. Achieved charging constraints for different budget values.

Note that 90% of chargers are busy means that CSs are at least 90% utilized and not underutilized.

Fig. 8 shows the effect of the increasing number of EVs on the minimum number of CSs required to achieve the target constraints: $\gamma_r = 0.1$ and $\gamma_d = 0.9$. As more EVs penetrate the market, more CSs will need to be planned so the technical charging constraints can be guaranteed. This result provides insights to operators who want to develop a CSs planning strategy to meet the charging demands of the anticipated penetrating number of EVs.

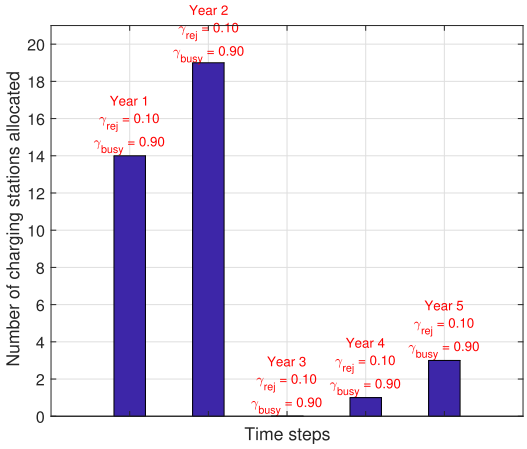

FIGURE 10. A graph showing the number of CSs allocated at each year for $T = 5$ and the corresponding rejection and non-idle charging levels achieved.

Next, we present the CSs allocation strategy given the spatio-temporal expansion of the power grid over 5 years. The expansion of the power grid and EVs is described by Algorithm 1 over a period of 5 years, i.e., $\mathcal{T} = \{1, 2, 3, 4, 5\}$. First, we need to find the budget limit that is required to achieve the target charging constraints ($\gamma_r = 0.1$ and $\gamma_d = 0.9$). Therefore, we plot in Fig. 9 the achieved rejection level, γ_r, and the achieved non-idle charging level, γ_d, for different budget values. We can see that a budget of \$250,000 is required to achieve the target charging constraints.

Next, we use the budget obtained in Fig. 9 to carry out the dynamic allocation of CSs over a period of 5 years. System operators have a CSs allocation plan as shown in Fig. 10 with a total budget of \$249,678.86, where for instance to meet the target charging constraints, 14 CSs need

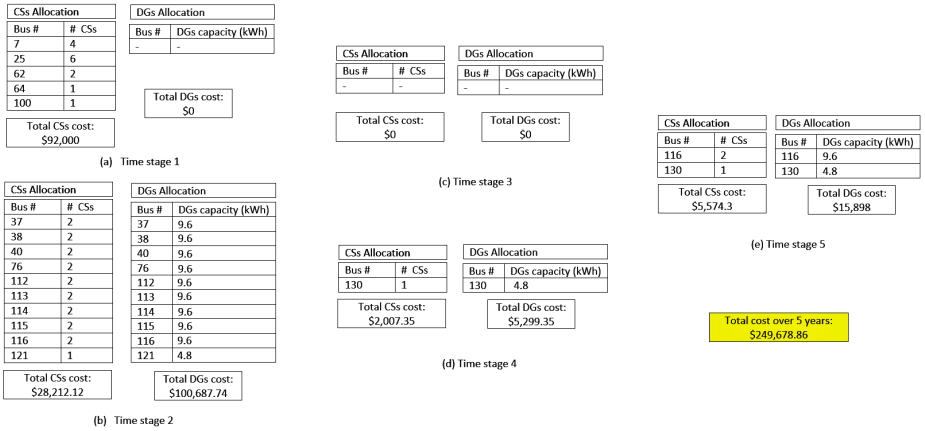

FIGURE 11. Tables showing the joint dynamic allocation of CSs and DGs with their corresponding bus numbers and their total costs for all the years of deployment.

to be initially installed at optimal locations in the first year, 19 additional CSs are needed for the second year, 1 CS for the fourth year, and 3 CSs for the fifth year. The exact locations for such CSs and their total costs are presented in Fig 11. As for DGs allocation, Fig. 11 shows the amount of DG capacity in kWh that is needed, its corresponding bus number and the total cost for the years of deployment. Note that the total cost at each stage depends on the number of deployed chargers.

Thus, operators can first determine the budget required to install both CSs and DGs based on the set technical constraints, and then input that budget into Algorithm 2 to solve the allocation strategy over a period of T years.

VI. CONCLUSION

In this paper, we have used stochastic geometry to model a spatio-temporal expanding grid that approximates common grid structures. Since the model's topological structure and characteristics evolve through time, it can be used as a powerful tool for any smart grid strategic planning.

The developed model was used to formulate a joint multi-year dynamic CSs and DGs allocation using a finite-horizon dynamic program. We carried out calculations to obtain lower-bound expressions on CSs density for acceptable charging service levels using stochastic geometry and queuing analysis. We then used these calculations to setup the dynamic program, which determined the number of CSs and DGs to allocate in each year given a budgetary constraint.

The results have revealed that the stochastic geometry-based power grid model approximates real-world power grids in terms of topological characteristics. Given some target charging constraints, system operators are equipped with three important pieces of information: i) the required budget that can be used over the planned deployment years for the purpose of allocating CSs and DG units, ii) the number and spatial locations of CSs and DG units in each year of the deployment plan, and iii) and a future insight on the number of required CSs to install after the deployment plan to meet the charging demands of a certain predicted number of penetrating EVs in the market. Thus, the model presented in this paper can be very useful for countries that require a more economical multi-stage expansion and deployment strategy to ease the integration of the increasing number of EVs.

Using the proposed stochastic geometry power grid model and a similar dynamic allocation algorithm, the allocation of swapping EV CSs for vehicle-to-vehicle (V2V) (dis)charging strategy will be studied as a direction for future research.

REFERENCES

[1] C. Beale. (2019). *Chart of the Day: China is Leading a Surge in Electric Vehicle Sales*. [Online]. Available: https://www.weforum.org/agenda/2018/05/china-surge-electric-vehicle-sales

[2] (2015). *Qatar Transitioning to Smart Meters*. [Online]. Available: http://www.qatarisbooming.com/article/qatar-transitioning-smart-meters

[3] A. S. A. Awad, M. F. Shaaban, T. H. M. EL-Fouly, E. F. El-Saadany, and M. M. A. Salama, "Optimal resource allocation and charging prices for benefit maximization in smart PEV-parking lots," *IEEE Trans. Sustain. Energy*, vol. 8, no. 3, pp. 906–915, Jul. 2017.

[4] N. Banol Arias, A. Tabares, J. F. Franco, M. Lavorato, and R. Romero, "Robust joint expansion planning of electrical distribution systems and EV charging stations," *IEEE Trans. Sustain. Energy*, vol. 9, no. 2, pp. 884–894, Apr. 2018.

[5] T. Courtat, C. Gloaguen, and S. Douady, "Mathematics and morphogenesis of cities: A geometrical approach," *Phys. Rev. E, Stat. Phys. Plasmas Fluids Relat. Interdiscip. Top.*, vol. 83, Mar. 2011, Art. no. 036106.

[6] D. Deka, S. Vishwanath, and R. Baldick, "Analytical models for power networks: The case of the Western U.S. and ERCOT grids," *IEEE Trans. Smart Grid*, vol. 8, no. 6, pp. 2794–2802, Nov. 2017.

[7] S. A. R. Zaidi and M. Ghogho, "Stochastic geometric analysis of black hole attack on smart grid communication networks," in *Proc. IEEE 3rd Int. Conf. Smart Grid Commun. (SmartGridComm)*, Nov. 2012, pp. 716–721.

[8] W. S. Kendall, "Geodesics and flows in a Poissonian city," *Ann. Appl. Probab.*, vol. 21, no. 3, pp. 801–842, Jun. 2011.

[9] T. Courtat, "Walk on city maps-mathematical and physical phenomenology of the city, a geometrical approach," Ph.D. dissertation, Dept. Phys., Paris Diderot Univ., Paris, France, 2012.

[10] C. Gloaguen, P. Coupe, R. Maier, and V. Schmidt, "Stochastic modelling of urban access networks," in *Proc. 10th Int. Telecommun. Netw. Strategy Planning Symp.* Munich, Germany: VDE e.V., Jun. 2002, pp. 99–104.

[11] Y. Ahn and H. Yeo, "An analytical planning model to estimate the optimal density of charging stations for electric vehicles," *PLoS ONE*, vol. 10, no. 11, Nov. 2015, Art. no. e0141307.

[12] Y. Gao and Y. Guo, "Optimal planning of charging station for phased electric vehicle," *Eastern Peripheral Expressway*, vol. 5, no. 4, pp. 1393–1397, 2013.

[13] J. Zhu, Y. Li, J. Yang, X. Li, S. Zeng, and Y. Chen, "Planning of electric vehicle charging station based on queuing theory," *J. Eng.*, vol. 2017, no. 13, pp. 1867–1871, Jan. 2017.

[14] M. F. Shaaban, S. Mohamed, M. Ismail, K. A. Qaraqe, and E. Serpedin, "Joint planning of smart EV charging stations and DGs in Eco–friendly remote hybrid microgrids," *IEEE Trans. Smart Grid*, vol. 10, no. 5, pp. 5819–5830, Sep. 2019.

[15] F. Baouche, R. Billot, R. Trigui, and N.-E. El Faouzi, "Efficient allocation of electric vehicles charging stations: Optimization model and application to a dense urban network," *IEEE Intell. Transp. Syst. Mag.*, vol. 6, no. 3, pp. 33–43, 2014.

[16] S. Cheng and P.-F. Gao, "Optimal allocation of charging stations for electric vehicles in the distribution system," in *Proc. 3rd Int. Conf. Intell. Green Building Smart Grid (IGBSG)*, Apr. 2018, pp. 1–5.

[17] R. M. Shukla and S. Sengupta, "A novel software-defined network based approach for charging station allocation to plugged-in electric vehicles," in *Proc. IEEE 16th Int. Symp. Netw. Computing Appl. (NCA)*, Oct. 2017, pp. 1–5.

[18] Y. Xiong, J. Gan, B. An, C. Miao, and A. L. C. Bazzan, "Optimal electric vehicle fast charging station placement based on game theoretical framework," *IEEE Trans. Intell. Transport. Syst.*, vol. 19, no. 8, pp. 2493–2504, Aug. 2018.

[19] F. Fleischer, F. Voss, V. Schmidt, and C. Gloaguen, "Distributional properties of Euclidean distances in wireless networks involving road systems," *IEEE J. Sel. Areas Commun.*, vol. 27, no. 7, pp. 1047–1055, Sep. 2009.

[20] Y. Jeong, J. Woon Chong, H. Shin, and M. Z. Win, "Intervehicle communication: Cox–fox modeling," *IEEE J. Sel. Areas Commun.*, vol. 31, no. 9, pp. 418–433, Sep. 2013.

[21] V. V. Chetlur and H. S. Dhillon, "Downlink coverage analysis for a finite 3d wireless network of unmanned aerial vehicles," *IEEE Trans. Commun.*, vol. 65, no. 10, pp. 4543–4558, Oct. 2017.

[22] S. Angel and A. M. Blei, "The spatial structure of American cities: The great majority of workplaces are no longer in CBDs, employment subcenters, or live-work communities," *Cities*, vol. 51, pp. 21–35, Jan. 2016.

[23] W. Kendall, "Networks and Poisson line patterns: Fluctuation asymptotics," *Oberwolfach Rep.*, vol. 5, no. 4, pp. 2670–2672, 2008.

[24] D. Deka, S. Backhaus, and M. Chertkov, "Structure learning in power distribution networks," *IEEE Trans. Control Netw. Syst.*, vol. 5, no. 3, pp. 1061–1074, Sep. 2018.

[25] S. H. Elyas, Z. Wang, and R. J. Thomas, "On the statistical settings of generation and load in a synthetic grid modeling," in *Proc. 10th Bulk Power Syst. Dyn. Control Symp. (IREP)*, Sep. 2017.
[26] S. Wagner, M. Götzinger, and D. Neumann, "Optimal location of charging stations in smart cities: A point of interest based approach," in *Proc. Int. Conf. Inf. Syst. (ICIS), Reshaping Soc. Through Inf. Syst. Design*, vol. 3, Jan. 2013, pp. 2838–2855.
[27] S. N. Chiu, D. Stoyan, W. S. Kendall, and J. Mecke, *Stochastic Geometry and Its Applications*. Hoboken, NJ, USA: Sep. 2013.
[28] V. V. Chetlur and H. S. Dhillon, "Coverage analysis of a vehicular network modeled as Cox process driven by Poisson line process," *IEEE Trans. Wireless Commun.*, vol. 17, no. 7, pp. 4401–4416, Jul. 2018.
[29] L. Zhang and Y. Li, "Optimal management for parking-lot electric vehicle charging by two-stage approximate dynamic programming," *IEEE Trans. Smart Grid*, vol. 8, no. 4, pp. 1722–1730, Jul. 2017.
[30] Y. Wang and J. S. Thompson, "Two-stage admission and scheduling mechanism for electric vehicle charging," *IEEE Trans. Smart Grid*, vol. 10, no. 3, pp. 2650–2660, May 2019.
[31] O. Hafez and K. Bhattacharya, "Integrating EV charging stations as smart loads for demand response provisions in distribution systems," *IEEE Trans. Smart Grid*, vol. 9, no. 2, pp. 1096–1106, Mar. 2018.
[32] A. Santos, *Summary of Travel Trends: 2009 National Household Travel Survey*. Washington, DC, USA: U.S. Department of Transportation, Federal Highway Administration, 2011.
[33] H. Liang, A. K. Tamang, W. Zhuang, and X. S. Shen, "Stochastic information management in smart grid," *IEEE Commun. Surveys Tuts.*, vol. 16, no. 3, pp. 1746–1770, 3rd Quart., 2014.
[34] I. S. Bayram, G. Michailidis, and M. Devetsikiotis, "Unsplittable load balancing in a network of charging stations under QoS guarantees," *IEEE Trans. Smart Grid*, vol. 6, no. 3, pp. 1292–1302, May 2015.
[35] H. Liang, I. Sharma, W. Zhuang, and K. Bhattacharya, "Plug-in electric vehicle charging demand estimation based on queueing network analysis," in *Proc. IEEE PES General Meeting Conf. Exposit.*, Jul. 2014, pp. 1–5.
[36] D. Ban, G. Michailidis, and M. Devetsikiotis, "Demand response control for PHEV charging stations by dynamic price adjustments," in *Proc. IEEE PES Innov. Smart Grid Technol. (ISGT)*, Jan. 2012, pp. 1–8.
[37] M. Ismail, I. S. Bayram, M. Abdallah, E. Serpedin, and K. Qaraqe, "Optimal planning of fast PEV charging facilities," in *Proc. 1st Workshop Smart Grid Renew. Energy (SGRE)*, Mar. 2015, pp. 1–6.
[38] D. Said, S. Cherkaoui, and L. Khoukhi, "Multi-priority queuing for electric vehicles charging at public supply stations with price variation," *Wireless Commun. Mobile Comput.*, vol. 15, no. 6, pp. 1049–1065, Apr. 2015, doi: 10.1002/wcm.2508.
[39] Y. Xu, W. Zhang, and W. Liu, "Distributed dynamic programming-based approach for economic dispatch in smart grids," *IEEE Trans. Ind. Informat.*, vol. 11, no. 1, pp. 166–175, Feb. 2015.
[40] L. Sankar, S. Rajagopalan, S. Mohajer, and H. Poor, "Smart meter privacy: A theoretical framework," *IEEE Trans. Smart Grid*, vol. 4, no. 2, pp. 837–846, Jun. 2013.
[41] N. Bäuerle and U. Rieder, *Markov Decision Processes With Applications to Finance*. Berlin, Germany: Springer-Verlag, 2011.
[42] L. C. M. Kallenberg, "Finite horizon dynamic programming and linear programming," *Methods Oper. Res.*, vol. 43, pp. 105–112, Jul. 1981.
[43] D. P. Bertsekas, *Dynamic Programming and Optimal Control*, 2nd ed. Belmont, MA, USA: Athena Scientific, 2000.
[44] D. Gleich. (2008). *MATLABbgl*. Accessed: Oct. 14, 2018. [Online]. Available: https://www.mathworks.com/matlabcentral/fileexchange/10922-matlabbgl
[45] F. Jamour, S. Skiadopoulos, and P. Kalnis, "Parallel algorithm for incremental betweenness centrality on large graphs," *IEEE Trans. Parallel Distrib. Syst.*, vol. 29, no. 3, pp. 659–672, Mar. 2018.
[46] I. Chadès, G. Chapron, M.-J. Cros, F. Garcia, and R. Sabbadin, "MDPtoolbox: A multi-platform toolbox to solve stochastic dynamic programming problems," *Ecography*, vol. 37, no. 9, pp. 916–920, Sep. 2014.
[47] R. Raustad, "Cost analysis of workplace charging for electric vehicles," Florida Solar Energy Center, Cocoa, FL, USA, Tech. Rep. FSEC-CR-2030-16, 2016.
[48] *Capital Cost Estimates for Utility Scale Electricity Generating Plants*, U.S. Energy Inf. Admin., Washington, DC, USA, Nov. 2016.

RACHAD ATAT (Member, IEEE) received the B.E. degree (Hons.) in computer engineering from Lebanese American University (LAU), Beirut, Lebanon, in 2010, the M.Sc. degree in electrical engineering from the King Abdullah University of Science and Technology (KAUST), Thuwal, Saudi Arabia, in 2012, and the Ph.D. degree (Hons.) in electrical engineering from the University of Kansas (KU), Lawrence, KS, USA, in 2017. He is currently a Postdoctoral Research Associate with Texas A&M University at Qatar, working on dynamic metering allocation with integrated cybersecurity measures in smart grids. His current research interests include smart grids, cybersecurity, and the Internet of Things. Dr. Atat was a recipient of the 2016 IEEE Global Communications Conference Best Paper Award, the NSF Travel Grant Award in 2016, the KU Engineering Fellowship Award, and the KAUST Discovery Award.

MUHAMMAD ISMAIL (Senior Member, IEEE) received the B.Sc. (Hons.) and M.Sc. degrees in electrical engineering (electronics and communications) from Ain Shams University, Cairo, Egypt, in 2007 and 2009, respectively, and the Ph.D. degree in electrical and computer engineering from the University of Waterloo, Waterloo, ON, Canada, in 2013. From 2013 to 2019, he was an Assistant Research Scientist with the Department of Electrical and Computer Engineering, Texas A&M University at Qatar. He is currently an Assistant Professor with the Department of Computer Science, Tennessee Tech University, Cookeville, TN, USA. His research interests include smart grids, wireless networks, and cyber-physical security. He was a co-recipient of the Best Paper Awards in the IEEE ICC 2014, the IEEE Globecom 2014, the SGRE 2015, the Green 2016, and the Best Conference Paper Award from the IEEE Communications Society Technical Committee on Green Communications and Networking at the IEEE ICC 2019. He was the Workshop Co-Chair in the IEEE Greencom 2018, the TPC Co-Chair in the IEEE VTC 2017 and 2016, the Publicity and Publication Co-Chair in the CROWNCOM 2015, and the Web-Chair in the IEEE INFOCOM 2014. He is an Associate Editor for the IEEE JOURNAL ON INTERNET-OF-THINGS, the IEEE TRANSACTIONS ON GREEN COMMUNICATIONS AND NETWORKING, *IET Communications,* and Elsevier PHYCOM. He was an Editorial Assistant of the IEEE TRANSACTIONS ON VEHICULAR TECHNOLOGY, from 2011 to 2013.

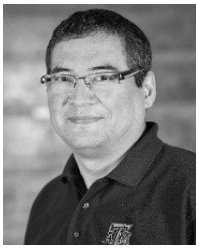

ERCHIN SERPEDIN (Fellow, IEEE) received the specialization degree in transmission and processing of information from Ecole Superieure D'Electricite, Paris, in 1992, the M.Sc. degree from the Georgia Institute of Technology, in 1992, and the Ph.D. degree from the University of Virginia, in January 1999. He is currently a Professor with the Department of Electrical and Computer Engineering, Texas A&M University, College Station. He is the author of two research monographs, one textbook, 17 book chapters, 160 journal articles, and 260 conference papers. His current research interests include signal processing, machine learning, cyber security, smart grids, bioinformatics, and wireless communications. He served as an Associate Editor for more than 12 journals and as a Technical Chair for six major conferences.

THOMAS OVERBYE (Fellow, IEEE) received the B.S., M.S., and Ph.D. degrees in electrical engineering from the University of Wisconsin-Madison. He is currently a TEES Eminent Professor with the Department of Electrical and Computer Engineering, Texas A&M University (TAMU). He has extensive experience in many aspects of electric power systems, including participating in or leading numerous large-scale electric grid studies.